Stabilities and defect-mediated lithium-ion conduction in a ground state cubic Li_3N structure

Manh Cuong Nguyen,*[1] Khang Hoang,[2] Cai-Zhuang Wang,[1] and Kai-Ming Ho[1]

[1]Ames Laboratory, U.S. DOE and Department of Physics and Astronomy, Iowa State University, Ames, IA 50011, USA

[2]Center for Computationally Assisted Science and Technology, North Dakota State University, Fargo, ND 58108, USA

Abstract

A stable ground state structure with cubic symmetry of Li_3N (c-Li_3N) is found by *ab initio* initially symmetric random-generated crystal structure search method. Gibbs free energy, calculated within quasi-harmonic approximation, shows that c-Li_3N is the ground state structure for a wide range of temperature. The c-Li_3N structure has a negative thermal expansion coefficient at temperatures lower than room temperature, due mainly to two transverse acoustic phonon modes. This c-Li_3N phase is a semiconductor with an indirect band gap of 1.90 eV within hybrid density functional calculation. We also investigate the migration and energetics of native point defects in c-Li_3N, including lithium and nitrogen vacancies, interstitials, and anti-site defects. Lithium interstitials are found to have a very low migration barrier (~0.12 eV) and the lowest formation energy among all possible defects. The ionic conduction in c-Li_3N is thus expected to occur via an interstitial mechanism, in contrast to that in the well-known α-Li_3N phase which occurs via a vacancy mechanism.

I. Introduction

Li_3N is known for being one of the highest ionic conducting materials.[1] The compound receives much attention due to its possible use as a Li-ion battery solid electrolyte, although the decomposition potential is too low for practical applications. Lithium vacancies in the Li_2N layer are responsible for the ionic conduction in the material.[1-3] Li_3N is considered as a promising material for hydrogen storage as well.[4,5] The compound is also known to be one of the most ionic nitrides as having nitrogen existing in N^{3-} state.[6,7]

Li_3N is well characterized in experiment as possessing a hexagonal structure with layers of Li_2N intercalated by Li,[8,9] namely P6/mmm α-Li_3N. Several theoretical studies have been carried out to investigate the electronic, defect, and transport properties of α-Li_3N.[2,3,7] Recent works show that α-Li_3N possesses imaginary phonon mode associated to the vibration along the c-axis of Li ion in the Li_2N plane. [3,7] This imaginary phonon mode would transform the α-Li_3N structure to the so-called P-3m1 α'-Li_3N structure. This transformation gains a very small energy for α'-Li_3N, –0.3 meV/atom in our calculation or –0.2 meV/atom in previous calculation.[3] The only difference of α'-Li_3N from α-Li_3N is that the Li ions in the Li_2N plane move out of the plane. The simulated x-ray diffraction patterns of α-Li_3N and α'-Li_3N are almost identical and a question on the identification of Li_3N structure in experiment might be raised.[3] Shen et. al.[10] very recently performed a systematic search for ambient and high pressure stable phases of Li-N binary by ab initio evolutionary algorithm. They found several new stable high pressure Li-N phases and presented a new high pressure phase diagram for Li-N system. At ambient condition, they found a cubic Li_3N structure having formation energy lower than those of α-Li_3N and α'-Li_3N structures.

In this work, we find the same low energy structure of Li_3N at ambient condition by random-generated crystal structure search method. Physical properties of the new Li_3N structure are intensively and comprehensively investigated. The Gibbs free energy of new Li_3N and α-Li_3N structures is calculated by taking into account vibrational entropy and thermal expansion effect within quasi-harmonic approximation. It is interesting that the thermal expansion coefficient of new Li_3N is negative at low temperature. The defect and migration calculations show that the lithium interstitial is the dominant native defect and its migration barrier is small, suggesting that new Li_3N could be a candidate for Li-ion conducting materials with interstitial mediated mechanism. The electronic, elastic and mechanical properties of new Li_3N are also investigated.

II. Computational methods

The first-principles density functional theory (DFT)[11] calculations are performed using Vienna *Ab Initio* Simulation Package (VASP)[12] with projector-augmented wave (PAW) pseudopotential method[13,14] within the generalized-gradient approximation (GGA) parameterized by Perdew, Burke, and Ernzerhof (PBE).[15] The energy cutoff is 550 eV and the Monkhorst-Pack's scheme[16] is used for Brillouin zone sampling. A high-quality k-point grid of $2\pi\times0.025$ Å^{-1}, equivalent to a k-point mesh of 10×10×10 for the below proposed structure, is used in all calculations. A twice denser k-point mesh is used for accurate density of states calculation. All structures are fully relaxed until the forces acting on each atom smaller than 0.01 eV/Å and pressure smaller than 1 kbar. The phonon frequencies are calculated by finite displacement method,[17] as implemented in the Phonopy code,[18] with forces calculated by VASP. The elastic constants are calculated using strain-stress relationship.[19] The band gap is also calculated with the hybrid functional parameterized by Heyd, Scuseria and Ernzerhof (HSE06).[20] The HSE06 functional has the standard mixing coefficient of 0.25 for the Hartree-Fock exchange energy in the exchange-correlation functional. The crystal structures for the HSE06 calculations are from GGA-PBE calculation. A half dense k-point mesh is used for hybrid functional calculations.

The references for formation energy and free energy calculations are the body-centered cubic Li metal and an N_2 molecule at 0 K. The dielectric constant is calculated by density functional perturbation theory.[21] A 3×3×3 supercell and a 4×4×4 k-point mesh are used in defect calculations for the below proposed structure of Li_3N. In these defect calculations, the atomic coordinates of defected structures are relaxed while the lattice parameters are kept fixed at the calculated bulk values. The defect formation energy is defined as[22]:

$$E_f(X^q) = E_{tot}(X^q) - E_{tot}(bulk) - \sum_i n_i\mu_i + q(E_v + \mu_e) + \Delta^q ,$$

where $E_{\mathrm{tot}}(X^q)$ is the total energy of a supercell containing a defect X in charge state q; E_{tot}(bulk) is the total energy of a supercell of the perfect bulk material; μ_i is the atomic chemical potential of species i (with reference to the bulk Li metal and N_2 molecule at 0 K) and n_i is the number of atom of species i that have been added ($n_i > 0$) or removed ($n_i < 0$) from the supercell of perfect bulk structure to form the defect; μ_e is the electron chemical potential, i.e., the Fermi level, referenced to the valence-band maximum in the bulk (E_v); Δ^q is the correction term to align the electrostatic potentials of the bulk and defect supercells and to account for the finite cell size effect on the total energy of charged defects. The atomic chemical potentials μ_i are subject to thermodynamic constraints, such as the condition for the stability of Li_3N:

$$3\mu_{\mathrm{Li}} + \mu_{\mathrm{N}} = \Delta H_f(\mathrm{Li_3N}),$$

where $\Delta H_f(\mathrm{Li_3N})$ is the formation energy of Li_3N; $\mu_{\mathrm{Li}} = 0$ ($\mu_{\mathrm{N}} = 0$) corresponds to extreme Li-rich (N-rich) conditions. Δ^q is estimated using the Freysoldt scheme,[23,24] which requires the value of the static dielectric constant. Our DFT calculation shows that the total static dielectric constant of the cubic Li_3N structure described below is $\varepsilon_0 = 6.76$. For comparison, the total static dielectric constant of α-Li_3N is calculated to be 13.05 (6.96) for $\varepsilon_0^{\perp}$ ($\varepsilon_0^{\parallel}$) component. The values for α-Li_3N are slightly above the upper limit or within the range for $\varepsilon_0^{\perp}$ and $\varepsilon_0^{\parallel}$ measured in experiment, which are 10.5 ± 1.5 and 6.0 ± 2.0, respectively. [25] The electronic contribution to the static dielectric constant of α-Li_3N is 6.05 (5.63) for $\varepsilon_\infty^{\perp}$ ($\varepsilon_\infty^{\parallel}$) in our calculation, in agreement with previous calculation.[3]

III. Results and discussion

A. Structural properties

For each unit cell size with 2, 3, 4, 6 and 8 formula units (f.u.) of Li_3N, 400 symmetrized structures are generated randomly. Once a space group is randomly selected from 230 available space groups, the lattice parameters in consistent with the chosen symmetry are generated and atoms are placed symmetrically within the unit cell by Wyckoff positions. The generated structures are then fully relaxed to local minima by DFT calculations. Through this random search, we find all the literature known structures of Li_3N. They include the known ground state α-Li_3N structure, recently proposed more stable α'-Li_3N structure and high pressure structures such as $P6_3/mmc$ β-Li_3N and Fm-3m γ-Li_3N. In addition, we find a Pm-3m cubic structure, hereafter called c-Li_3N, with formation energy lower than all known structures at ambient condition. The c-Li_3N phase has a formation energy of –1.621 eV/f.u., which is 26 or 25 meV/f.u. lower than that of α- or α'-Li_3N, respectively. In our DFT calculation, the formation energy of α-Li_3N is –1.595 eV/f.u., in agreement with previous calculations[2] and slightly smaller than the experimental value.[26] The c-Li_3N is the same with new Li_3N structure reported recently by Shen et. al.[10]

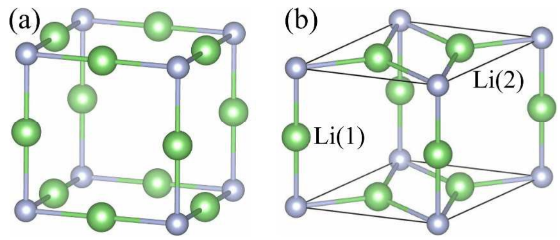

Figure 1. Crystal structures of (a) c-Li_3N and (b) α-Li_3N with large (green) balls representing Li atoms and small (grey) balls representing N atoms.

Table I. Lattice constants and Li–N bond lengths of c-Li_3N, α-Li_3N and α'-Li_3N structures from our DFT calculations, previous DFT calculations and experiment.

		a (Å)	*c* (Å)	Li(1)-N / Li(2)-N (Å)
c-Li_3N		3.874		1.937
α-Li_3N				
	This work	3.634	3.869	1.934 / 2.098
	Ref. 3	3.640	3.871	1.936 / 2.102
	Experimental[a]	3.648	3.875	1.938 / 2.106
α'-Li_3N				
	This work	3.629	3.871	1.936 / 2.101
	Ref. 3	3.635	3.871	1.936 / 2.102

[a]Reference [8].

We list in Table I the lattice parameters of c-Li_3N as well as those of α-Li_3N and α'-Li_3N. The calculated values for α-Li_3N and α'-Li_3N are in agreement (within 1%) with those from other calculations and experiments.[2,3,7,8] The c-Li_3N structure possesses the Pm-3m symmetry with Li occupying the 3*d* Wyckoff position and N occupying the 1*a* Wyckoff position. Figure 1 shows the crystal structures of c-Li_3N and α-Li_3N. In α-Li_3N, Li(1) and Li(2) ions have coordination numbers of 2 and 8, respectively, and N ions are coordinated by 8 Li ions; in c-Li_3N, on the other hand, all Li ions are coordinated by 2 N ions and N ions are coordinated by 6 Li ions. This lower coordination of both Li and N ions is responsible for an interesting fact that the volume per atom of c-Li_3N is much larger (~30%) than that of α-Li_3N. They are 14.54 and 11.06 $Å^3$/atom for c-Li_3N and α-Li_3N, respectively. If a negative pressure can be applied on Li_3N, the stability of c-Li_3N would be enhanced significantly by the advance of PV term contribution to formation enthalpy H = E + PV, where E is the internal energy, P is pressure and V is volume. In the other words, this c-Li_3N would be synthesized easier with experimental techniques which can employ negative pressure.

B. Thermodynamic, dynamic and mechanical stabilities

We calculate the phonon spectrum of c-Li_3N to investigate its dynamical stability. Figure 2 shows the phonon spectra of c-Li_3N and α-Li_3N along the high symmetry points of the c-Li_3N and α-Li_3N Brillouin zones. The α-Li_3N structure shows a negative phonon frequency around the Γ point, which is consistent with previous calculations and implies a dynamical instability of α-Li_3N as pointed out in previous works.[3,7] In contrast, c-Li_3N does not possess any negative phonon frequency, indicating that this structure is dynamically stable. This result is consistent with previous work.[10]

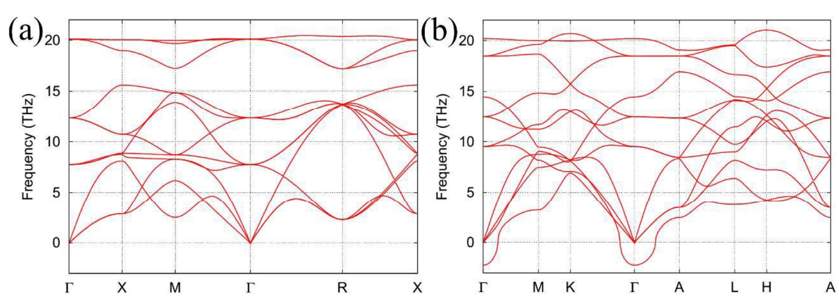

Figure 2. Phonon spectra of (a) c-Li_3N and (b) α-Li_3N structures.

Table II shows the calculated elastic constants and moduli of c-Li_3N. The elastic constants are calculated based on strain-stress relationships and the bulk, shear and Young moduli are calculated from elastic constants using the Voigt-Reuss-Hill approximation.[27] We find that the elastic constants of c-Li_3N satisfy the following Born stability criteria[28]:

$$C_{11} - C_{12} > 0,\ C_{11} + 2C_{12} > 0,\ C_{44} > 0.$$

The c-Li_3N structure is thus mechanically as well as dynamically stable. We note that in our calculations the elastic constants of both α- and α'-Li_3N satisfy the corresponding Born stability criteria for the hexagonal crystal.

Table II. The elastic constants (C_{ij}), bulk (B), shear (G) and Young (Y) moduli in the unit of GPa for c-Li_3N structure.

C_{11}	C_{12}	C_{33}	C_{44}	B	G	Y
112.4	5.6	112.4	13.7	41.2	24.5	61.3

We also perform Gibbs free energy calculation for c-Li_3N and α'-Li_3N within the quasi-harmonic approximation to investigate the change of structures and their relative stabilities with temperature. Because α-Li_3N is not dynamically stable, at least in our calculations and those reported in the literature, we use α'-Li_3N in the Gibbs free energy calculation in the place of α-Li_3N. The α-Li_3N and α'-Li_3N structures are almost identical as mentioned above so we assume that the thermal properties of α-Li_3N and α'-Li_3N are very similar. Phonon frequencies of c-Li_3N and α'-Li_3N at different scaled volumes, from 96% to 112% of the equilibrium volume with 26 equally spacing sampling volume points, are calculated to get the Helmholtz free energies as a function of unit cell volume. The temperature effect is taken into account via vibrational (phonon) entropy. The Vinet equation of state then is used to fit the Helmholtz energy curve at each temperature. The Gibbs free energy is obtained from Helmholtz free energy by a Legendre transform. Figure 3(a) shows the calculated Gibbs free energies of c-Li_3N and α'-Li_3N. It is clear that c-Li_3N is always more stable than α'-Li_3N in the whole range of temperature under consideration, from 0 to 600 K. This result, together with the above discussed thermodynamic and dynamical stabilities, show that c-Li_3N is indeed the ground state structure of Li_3N in a wide range of temperature. However, all experiments up to now have observed α-Li_3N as the stable structure of Li_3N at ambient condition. There could be a kinetic barrier blocking the formation of c-Li_3N, making α-Li_3N more favorable within the experimental synthesis techniques having been used so far to synthesize Li_3N. On the other hand, experiment showed that α-Li_3N contains close to 3% of Li vacancy, mostly at the Li(2) site, at room temperature.[9] Previous calculation also show that the formation energy of Li(2) vacancies is low.[2] These observation and calculation results imply that off-stoichiometry could be another driving force in favor the formation of α-Li_3N instead of c-Li_3N at ambient condition although c-Li_3N is more thermodynamically stable.

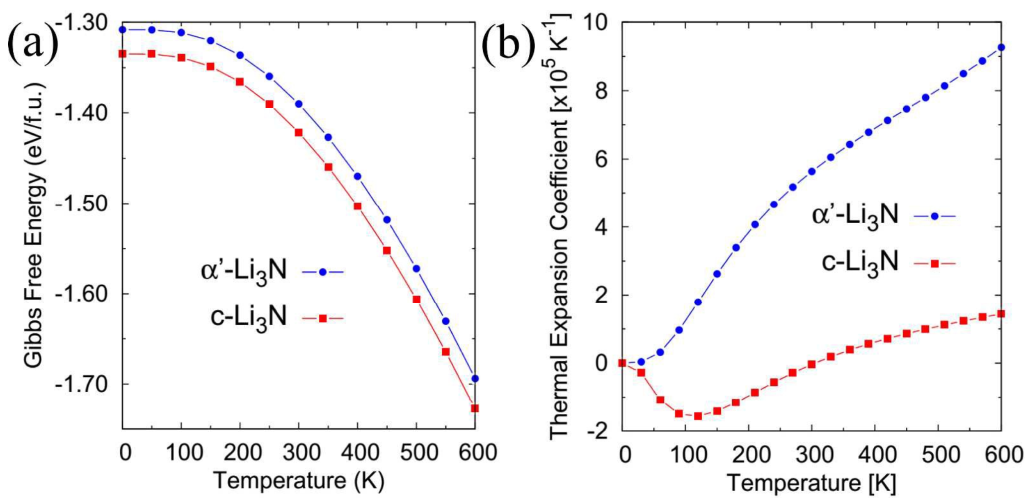

Figure 3. (a) Gibbs free energies and (b) thermal expansion coefficients of c-Li_3N and α'-Li_3N structures as a function of temperature.

From the Helmholtz free energy calculations, we can extract the temperature dependences of the unit cell volumes of c-Li_3N and α'-Li_3N and hence their thermal expansion coefficients as a function of temperature. For comparison, the thermal expansion coefficient of α-Li_3N is 3.5×10^{-5} K^{-1} at 300 K as observed in experiment by fitting to refined lattice parameters from neutron diffractions at different temperatures.[29] The thermal expansion coefficient of α'-Li_3N in our calculation is 5.6×10^{-5} K^{-1}. As mentioned above, α-Li_3N has negative phonon frequencies therefore α'-Li_3N is used for comparisons with experimental data. Although the comparison may not be direct, it shows that our calculations are reliable and the results are comparable with experimental observations. Figure 3(b) shows the thermal expansion coefficients of c-Li_3N and α'-Li_3N as a function of temperature. Interestingly, c-Li_3N is found to have a negative thermal expansion coefficient at temperature lower than room temperature. The thermal expansion coefficient of α'-Li_3N is always positive in the whole range of considered temperature. The negativity of thermal expansion coefficient of c-Li_3N implies that the newly identified structure could be used as a functional material for controllable thermal expansion composite to tailor the expansion coefficient to a desired value for using in applications like high precise optical mirrors, fiber optic systems, electronics, low temperature sensing or even in dental fillings.[30,31] Our mode Grüineisen parameter calculations for different phonon modes show that two transverse acoustic phonon modes have much more negative Grüineisen parameters than other phonon modes. The mode Grüineisen parameters of these two transverse acoustic phonon modes along the q-path from Γ to X points are negative and can be as low as –41. At low temperatures where only acoustic modes are excited, the negativity of mode Grüineisen parameters of these two acoustic modes is mainly responsible for the negative thermal expansion of c-Li_3N. The same phenomenon was found in the well-known negative thermal expansion material ZrW_2O_8, where the transverse vibrations of the Zr-O-W linkage between WO_4-tetrahedron and ZrO_6-octahedron are responsible for the negative thermal expansion.[32-34] Huang et al recently generalized the origin of negative thermal expansion of water/ice to suggest that the negative thermal expansion of a material is resulting from the evolvement of the disparity of interactions such as the strong O-H bond and weak O:H non-bond in water/ice.[34] In the c-Li_3N (ZrW_2O_8) system, the strong Li-N bonding within NLi_6-octahedron (W-O bonding within WO_4-tetrahedron and Zr-O bonding within ZrO_6-octahedron) and the rotational vibration of the octahedron (tetrahedron and octahedron) induced by the transverse vibration of the bridging Li (O) atom play very much the roles of strong O-H bond and weak O:H non-bond in the generalized model for negative thermal expansion.[34]

Before considering the electronic properties, let us consider the bonding character of c-Li_3N. We perform Bader charge analysis[35] for both α-Li_3N and c-Li_3N. The charges associated with Li (N) ions are +0.83 |e| (–2.49 |e|) in both α-Li_3N and c-Li_3N, compared to the formal charges of +1 |e| (–3 |e|), showing that the bonding in c-Li_3N is strongly ionic as in α-Li_3N.[6]

C. Electronic properties

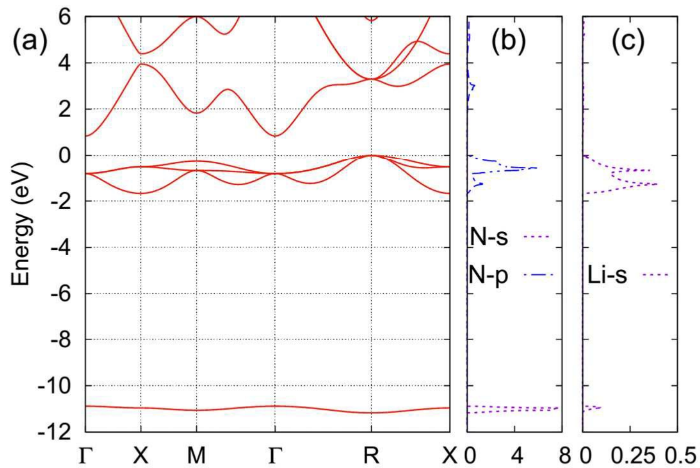

Figure 4. Electronic (a) band structure and (b, c) projected density of states (states/eV/unit cell) of c-Li_3N. The zero of energy is set to the highest occupied state.

Figure 4 shows the electronic band structure along the lines connecting high symmetric *k*-points of the Brillouin zone and the projected density of states of c-Li_3N. The c-Li_3N structure is indirect semiconducting with the valence-band maximum (VBM) at the R point and the conduction-band minimum (CBM) at the Γ point. The band gap is 0.85 eV from our GGA calculation. However, it is well known that GGA underestimates the band gap of semiconductors and insulators. So we perform HSE06 hybrid functional calculation[16] for c-Li_3N structure obtained from GGA calculation to get a better description of the energy band gap. Our HSE06 calculation shows that the band gap of c-Li_3N is 1.90 eV. For comparison, the HSE06 band gap of α-Li_3N is 2.07 eV in our calculation, in good agreement with the experimental value of 2.18 eV.[36] As can be seen in Fig. 4, the N 2*s* band lies very deep below the Fermi level, which is similar to the N 2*s* band in α-Li_3N.[2] There is a small hybridization between Li 1*s* and 2*s* orbitals with N 2*s* orbitals at this energy level. The contribution of N to the occupied states near the VBM is almost solely from the N 2*p* orbitals. The contribution from Li 2*s* orbital to occupied states near the VBM is small in comparison to that from N 2*p* orbitals. The unoccupied states near CBM are mainly from N 2*p* orbital. These results are consistent with previous work.[10]

D. Defects and Lithium-ion conduction

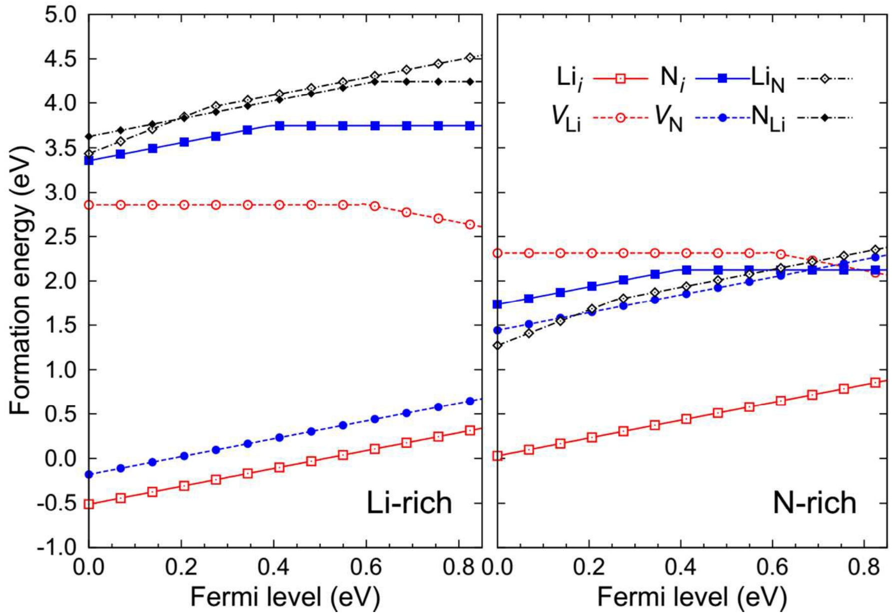

Figure 5. Formation energies of native defects in c-Li_3N under Li-rich and N-rich conditions, plotted as function of Fermi level with respect to the VBM.

The Li vacancy at the Li(2) position is identified responsible for the charge carriers in high ionic conducting α-Li_3N.[1] Previous defect calculations[2] also show that lithium vacancies at the Li(2) site in α-Li_3N have the lowest formation energy under N-rich condition. In the present work, we calculate the formation energies of native defects in the newly identified c-Li_3N structure. Figure 5 shows the calculated formation energies of lithium and nitrogen vacancies (V_{Li} and V_N), interstitials (Li_i and N_i), and anti-site defects (Li_N and N_{Li}) in different charge states. We find that the positively charged lithium interstitial Li_i^+ is the defect with the lowest formation energy in the entire range of the Fermi-level values, under both the Li-rich and N-rich conditions, indicating that it is the dominant native defect in c-Li_3N. This interstitial is most stable at a position 0.49 Å off the center and on the diagonal line of a cubic unit cell surface, which has local environment quite similar to that of Li(2) in α-Li_3N [see Fig. 1(b)]. Since Li_i^+ has a low formation energy and hence can occur with a high concentration, more lithium can be incorporated into c-Li_3N, making it a high-capacity lithium storage medium. Besides, given that Li_i^+ is a shallow donor, see Fig. 5, this defect can lead to n-type conductivity. The positively charged nitrogen vacancy V_N^+ also has a low formation energy under the extreme Li-rich condition. The formation energy of V_{Li}^0 is about 2.3 eV under the extreme N-rich condition, comparable to that of the lithium vacancy at the Li(1) site in α-Li_3N reported by Wu et al.[2]

Finally, we find a metastable structure for the lithium Frenkel pair, (Li_i^+,V_{Li}^-), that has a formation energy of 1.64 eV and a binding energy of 1.39 eV; the distance between the two components of the pair is 2.09 Å.

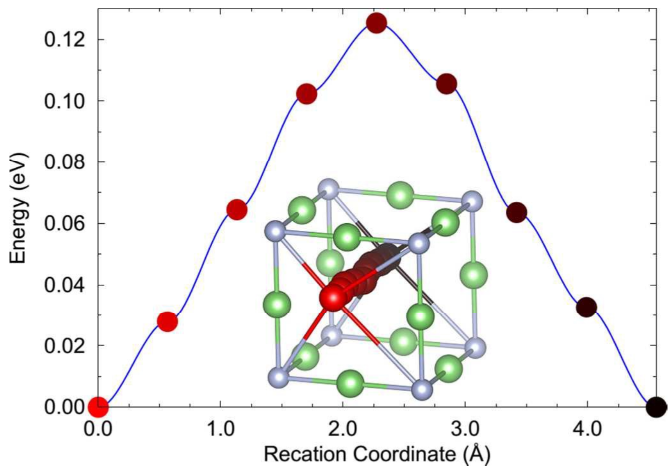

Figure 6. Migration path and barrier for Li_i^+. Red to black balls represent the Li_i^+ along the migration path.

Lithium migration in c-Li_3N is investigated using the climbing-image nudged elastic-band method (NEB).[37] The NEB calculations are performed with a same 3×3×3 supercell with that of defect calculations. Figure 6 shows a schematic picture of the migration path (within a single unit cell only) and the calculated migration barrier of Li_i^+. The migration barrier is about 0.12 eV for Li_i^+. For comparison, the migration barrier of V_{Li}^- is calculated to be 0.46 eV. Given the much lower formation energy and migration barrier associated with Li_i^+, it is expected that the ionic conduction in c-Li_3N proceeds via the interstitial mechanism. This is in contrast to α-Li_3N where ionic conduction occurs through a vacancy mechanism.[1]

IV. Conclusions

In summary, we have identified a cubic ground state structure of Li_3N, namely c-Li_3N. The Gibbs free energy of c-Li_3N is always lower than that of α'-Li_3N in the considered temperature range from 0 to 600 K. The c-Li_3N structure is also dynamically and mechanically stable again thermal vibration and mechanical distortion. Its thermal expansion coefficient is negative at low temperatures and the negativity of mode Grüineisen parameters of two transverse acoustic modes is mainly responsible for this negative thermal expansion. The cubic phase is semiconducting with an indirect energy band gap of 1.90 eV. Amongst possible native defects, the lithium interstitial is dominant in c-Li_3N and its migration barrier is small, implying that the ionic conduction in c-Li_3N is interstitial mediated.

Acknowledgements

This work was supported by the U.S. Department of Energy (DOE), Office of Science, Basic Energy Sciences, Materials Science and Engineering Division, including computing time at the National Energy Research Scientific Computing Center (NERSC). The research was performed at the Ames Laboratory, which is operated for the U.S. DOE by Iowa State University under contract # DE-AC02-07CH11358. K. H. was supported by the U.S. Department of Energy Grant No. DE-SC0001717.

*Email: mcnguyen@ameslab.gov

References

1. U. v. Alpen, J. *Solid State Chem.*, 1979, **29**, 379.
2. S. Wu, Z. Dong, F. Boey, and P. Wu, *Appl. Phys. Lett.*, 2009, **94**, 172104.
3. G. Wu, S. Wu, and P. Wu, *Phys. Rev. Lett.*, 2011, **107**, 118302.
4. P. Chen, Z. Xiong, J. Luo, J. Lin, and K. L. Tan, *Nature*, 2002, **420**, 302.
5. T. Ichikawa, S. Isobe, N. Hanada, and H. Fujii, *J. Alloys Compd.*, 2004, **365**, 271.
6. H. Schulz, and K. Schwarz, *Acta Crystallogr. Sect. A*, 1978, **34**, 999 (1978).
7. Y. Yan, J. Y. Zhang, T. Cui, Y. Li, Y. M. Ma, J. Gong, Z. G. Zong, and G. T. Zou, Eur. *J. Phys. B*, 2008, **61**, 392.
8. H. J. Beister, S. Haag, R. Kniep, K. Strossner, and K. Syassen, *Angew. Chem. Int. Ed. Engl.*, 1988, **27**, 1101.
9. D. H. Gregory, P. M. O'Meara, A. G. Gordon, J. P. Hodges, S. Short, and J. D. Jorgensen, *Chem. Mater.*, 2002, **14**, 2063.
10. Y. Shen, A. R. Oganov, G. Qian, J. Zhang, H. Dong, Q. Zhu, and Z. Zhou, *Sci. Rep.*, 2015, **5**, 14204.
11. W. Kohn and L. J. Sham, *Phys. Rev.*, 1965, **140**, A1133.
12. G. Kresse and J. Furthmüller, *Comput. Mat. Sci.*, 1996, **6**, 15.
13. P. E. Blochl, *Phys. Rev. B*, 1994, **50**, 17953.

14. G. Kresse and D. Joubert, *Phys. Rev. B*, 1999, **59**, 1758.
15. J. P. Perdew, K. Burke, and M. Ernzerhof, *Phys. Rev. Lett.*, 1996, **77**, 3865.
16. H. J. Monkhorst and J. D. Pack, *Phys. Rev B*, 1976, **13**, 5188.
17. K. Parlinski, Z. Q. Li, and Y. Kawazoe, *Phys. Rev. Lett.*, 1997, **78**, 4063.
18. A. Togo, F. Oba, and I. Tanaka, *Phys. Rev. B*, 2008, **78**, 134106.
19. Y. Le Page and P. Saxe, *Phys. Rev. B*, 2002, **65**, 104104.
20. J. Heyd, G. E. Scuseria, and M. Ernzerhof, *J. Chem. Phys.*, 2006, **124**, 219906.
21. M. Gajdoš, K. Hummer, G. Kresse, J. Furthmüller, and F. Bechstedt, *Phys. Rev. B*, 2006, **73**, 045112.
22. C. Freysoldt, B. Grabowski, T. Hickel, J. Neugebauer, G. Kresse, A. Janotti, and C. G. Van de Walle, *Rev. Mod. Phys.*, 2014, **86**, 253.
23. C. Freysoldt, J. Neugebauer, and C. G. Van de Walle, *Phys. Rev. Lett.*, 2009, **102**, 016402.
24. C. Freysoldt, J. Neugebauer, and C. G. Van de Walle, *Phys. Status Solidi B*, 2011, **248**, 1067.
25. H. R. Chandrasekar, G. Bhattacharya, R. Minogi, and H. Bilz, *Phys. Rev. B*, 1978, **17**, 884.
26. J. M. McHale, A. Navrotsky, G. R. Kowach, V. E. Balbarin, and F. J. DiSalvo, *Chem. Mater.*, 1997, **9**, 1538.
27. R. Hill, Proc. *Phys. Soc. A*, 1952, **65**, 350.
28. F. Mouhat and F.-X. Coudert, *Phys. Rev. B*, 2014, **90**, 224104.
29. A. Huq, J. W. Richardson, E. R. Maxey, D. Chandra, and W.-M. Chien, *J. Alloys. Compd.*, 2007, **446**, 256.
30. J. Chen, L. Hu, J. Deng, and X. Xing, *Chem. Soc. Rev.*, 2015, **44**, 3522.
31. J. S. O. Evans, *J. Chem. Soc. Dalton Trans.*, 1999, **19**, 3317.
32. A. K. A. Pryde, K. D. Hammonds, M. T. Dove, V. Heine, J. D. Gale, M. C. Warren, *J. Phys.: Condens. Matter*, 1996, **8**, 10973.
33. T. A. Mary, J. S. O. Evans, T. Vogt, and A. W. Sleight, *Science*, 1996, **272**, 90.
34. Y. Huang, X. Zhang, Z. Ma, Y. Zhou, W. Zheng, J. Zhou, and C. Q. Sun, *Coord. Chem. Rev.*, 2015, **285**, 109.
35. G. Hankelman, A. Arnardsson, and H. Jónsson, *Comput. Mater. Sci.*, 2006, **36**, 254.

36. H. Brendecke and W. Bludau, *Phys. Rev. B*, 1980, **21**, 805.

37. G. Henkelman, B. P. Uberuaga, and H. Jónsson, *J. Chem. Phys.*, 2000, **113**, 9901.